NANO LETTERS
Cite This: Nano Lett. 2018, 18, 3850−3856
Letter
pubs.acs.org/NanoLett

Direct Observation of Large Flexoelectric Bending at the Nanoscale in Lanthanide Scandates

Pratik Koirala, Christopher A. Mizzi, and Laurence D. Marks*

Department of Materials Science and Engineering, Northwestern University, Evanston, Illinois 60208, United States

Supporting Information

ABSTRACT: There is a growing interest in the flexoelectric effect, since at the nanoscale it is predicted to be very large. However, there have been no direct observations of flexoelectric bending consistent with current theoretical work that implies strains comparable to or exceeding the yield strains of typical materials. Here we show a direct observation of extraordinarily large, two-dimensional reversible bending at the nanoscale in dysprosium scandate due to the converse flexoelectric effect, with similar results for terbium and gadolinium scandate. Within a transmission electron microscope, thin features bend up to 90° with radii of curvature of about 1 μm, corresponding to very large nominal strains. Analysis including independent experimental determination of the flexoelectric coefficient is semiquantitatively consistent with interpreting the results as due to flexoelectricity. These results experimentally demonstrate large flexoelectric bending at the nanoscale.

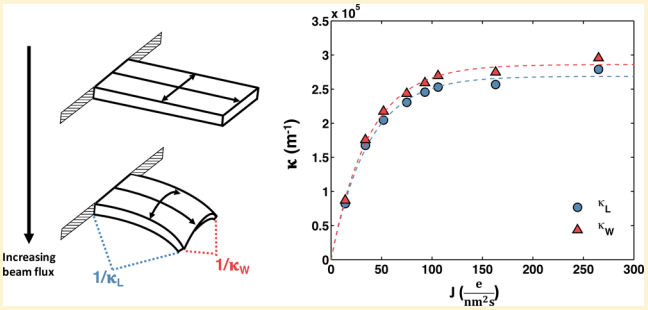

KEYWORDS: *Flexoelectricity, in situ, transmission electron microscopy, lanthanide scandates*

Higher order electromechanical couplings in materials are an area of substantial current research since they involve spatial gradients of applied fields which activate traditionally forbidden responses, such as mechanically induced polarization in centrosymmetric materials. One of these is the flexoelectric effect, which couples polarization and strain gradient. Though typically small at the macroscale, the size scaling of strain gradients is expected to lead to large flexoelectric responses at the nanoscale. Understanding the fundamental science of this phenomenon will help expedite its inclusion in existing devices and could open possibilities for new applications.

First observed in solids by Bursian and Zaikovskii,[1] the term flexoelectricity was coined in the field of liquid crystals[2] and subsequently adopted for solids[3] and also biological membranes.[4] The current resurgence of interest in the flexoelectric effect in oxide systems,[5,6] largely sparked by measurements made by Cross and Ma on relaxor ferroelectrics,[7] has led to major experimental[8−11] and theoretical[12−18] progress in understanding flexoelectricity. From these experimental and theoretical advances, it has been found that flexoelectric couplings in oxides have profound impacts on mechanical[19,20] and dielectric[21,22] properties, can change domain walls and interfaces in ferroelectrics[23−26] and ferroelastics,[27,28] and can control defect formation,[29] among many other discoveries. Advances in our understanding of this phenomenon have led to a number of promising applications including flexoelectric energy harvesting,[30,31] actuation,[32] and strain sensing.[33] Improving the efficacy of flexoelectric-based devices requires advancing the understanding of the underlying science of flexoelectricity.

In their pioneering work, Bursian and Zaikovskii[1] observed curvature in a $BaTiO_3$ film due to the application of an electric field. A 2.5 μm thick film of $BaTiO_3$ was measured to have a curvature of 150 m^{-1} under an applied potential of 20 V. In films of nanometer thickness, it was predicted that the curvature would be on the order of 10^6 to 10^{10} m^{-1}, which equates to strains comparable to or exceeding typical oxide yield strains. This occurs because the flexural rigidity of a plate scales as the elastic thickness cubed, dropping precipitously at small sizes. None of the existing literature includes direct experimental evidence demonstrating the predicted high curvature and strain values, although there are some indirect measurements of comparable curvatures (e.g., ref 34). A subtle question is whether such large effects are physically realistic or just nominal extrapolations.

In this Letter, we report direct experimental observations of large, two-dimensional reversible flexoelectric bending at the nanoscale in $DyScO_3$ with similar results for $TbScO_3$ and $GdScO_3$. Within a transmission electron microscope (TEM), thin features of these single crystal oxides bend up to 90° with radii of curvature ∼1 μm when positively charged by the loss of secondary electrons. The bending scales with electron beam flux and is not associated with any dislocations, twinning, or

Received: March 20, 2018
Revised: May 10, 2018
Published: May 14, 2018

DOI: 10.1021/acs.nanolett.8b01126
Nano Lett. 2018, 18, 3850−3856

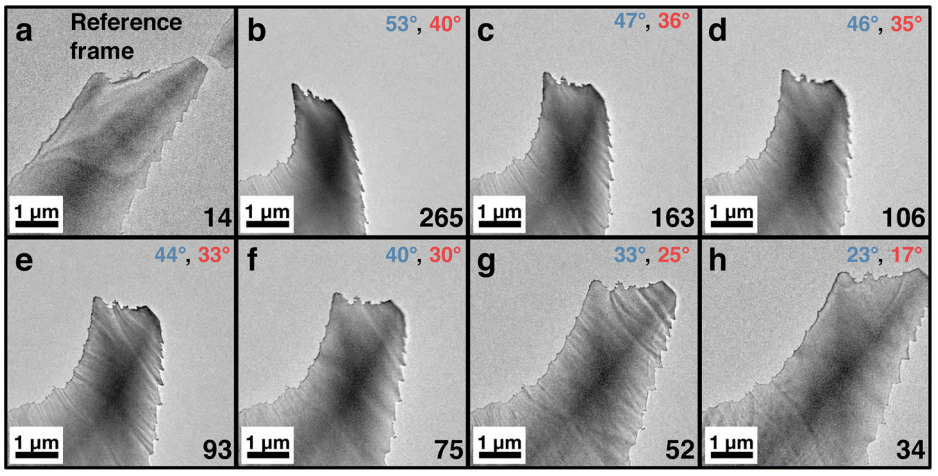

Figure 1. Downward bending of a [110] oriented $DyScO_3$ sample under the electron beam. Eight frames taken from Video V1 in the Supporting Information show a decrease in the downward bending of the sample as flux is decreased from panels b–h. The approximate electron flux (electrons/nm^{2}s) is given in the bottom right corner of each frame. The bending angles along the length (blue) and width (red) of the feature given at the top right corner of each frame are calculated from the projected dimensions with respect to the unbent reference frame in panel a.

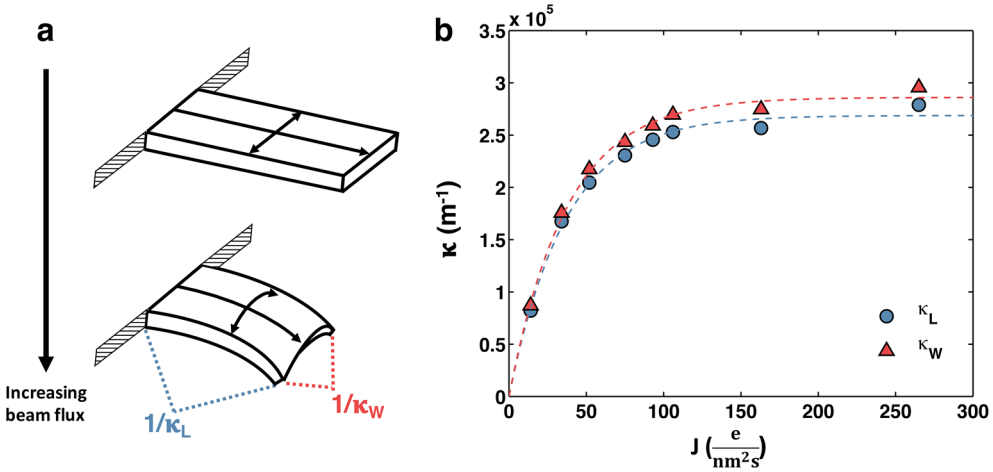

Figure 2. Curvature under exposure to the electron beam. (a) Illustration of a sample bending in response to an increasing beam flux. A bent sample exhibits curvature along its length (κ_L) and width (κ_W). For simplicity, the features observed in TEM are drawn as black cantilevers. (b) Curvature (κ) along the length and width of the feature in Figure 1 is plotted as a function of incident electron beam flux (J).

similar changes in the oxide. Extensive additional analyses of these materials to better define the source of this bending are presented, including atomic force microscopy (AFM), X-ray photoelectron spectroscopy (XPS), ultraviolet photoelectron spectroscopy (UPS), reflection electron energy loss spectroscopy (REELS), ex situ measurements of flexoelectric coefficients, and theoretical modeling using density functional theory (DFT) with hybrid exact-exchange functionals. The results semiquantitatively indicate that the observed bending is a consequence of large charging coupled to curvature via a high flexocoupling voltage. In most cases, the magnitude of the bending is not limited by yield strength, but by the achievable potential across the oxide as set by the band gap in the limit of a thin insulator.

Figure 1 shows a number of frames from Video V1 in the Supporting Information, in which a thin $DyScO_3$ sample bends under the illumination of a TEM electron beam. Increasing the electron flux by converging the beam increased bending, while decreasing the electron flux had the opposite effect. If the electron beam was not centered on the sample, it bent away from the beam (Supporting Information, Figure S1 and Video V2). In general, the bending was reversible, although too severe bending could cause fracture (Supporting Information, Video V3).

While bending along the length of the sample is clearest in Figure 1, it was definitively two-dimensional, occurring along both the length and width of the sample. As the electron flux was increased, the sample shape approached that of a spherical zone. An illustration of this two-dimensional bending is shown in Figure 2a. By comparing the projected length and width of the sample in Figure 1 at various fluxes to the reference frame (lowest flux used), we extracted the curvature along the sample length and width as a function of flux. As shown in Figure 2b, the relationship between flux, estimated assuming a quantum yield of 0.2, and curvature is well described by an empirical fit of the form $\kappa = A\left(1 - \exp\left(-\frac{J}{B}\right)\right) + \kappa_0$ where κ is the curvature, J is the flux, A and B are constants, and κ_0 is the (unmeasured) curvature of the reference frame. This implies saturation of the curvature as a function of flux and, as discussed later, is consistent with saturation of sample charging as a function of flux.

DOI: 10.1021/acs.nanolett.8b01126
Nano Lett. 2018, 18, 3850–3856

Despite using electron fluxes on the order of 1−100 electrons/nm^{2}s, which are significantly lower than electron fluxes typically used for high resolution imaging or chemical analysis at the nanoscale with electron microscopes (10^4 to 10^6 electrons/nm^{2}s), there was considerable sample charging. To confirm that charging was linked to the observed bending, a sample was coated with a thin layer of carbon (a common charge passivation technique). As charging was nonexistent with the carbon coating and the bending was minimal to none, the charging and bending in our experiments are linked. In a related test, a low energy ion-beam mill was used to disorder the surface of a $DyScO_3$ sample. After the surface was disordered, the charging was less severe and the bending was minimal to none. This indicates that the surface plays some role in the observed charging and bending.

The bending and associated charging were observed for about 50 different features from 20 different samples, including $TbScO_3$ and $GdScO_3$ samples. We did not observe any dependence upon the crystallographic direction of the features with the caveat that the thin direction was always [110]. The process appeared to be elastic with no evidence of dislocations or phase transitions and was often on the time scale of the video recordings. We looked for similar charging and bending in $SrTiO_3$, $KTaO_3$, $NdGaO_3$, and $LaAlO_3$. There was some charging in $NdGaO_3$ and $LaAlO_3$ (significantly less than in the lanthanide scandates), but little to no bending.

Our observations indicate that the curvature in the $DyScO_3$ samples saturates as a function of flux, the bending is a consequence of large charging in this material, and the nature of the surface plays some role in the charging. Now we turn to establishing the origin of this charging, the role of the surface, and how these observations are attributed to the converse flexoelectric effect.

For high incident electron energies (as typically used in TEM) charging in insulators will be net positive, involving the loss of secondary electrons. The charging will scale with the electron flux and be partially compensated by competing neutralization processes, such as the capture of secondary electrons from other locations in the microscope. The spatial distribution of this charge does not have to be symmetric, and in fact, one would anticipate the top surface of the sample to charge positive with respect to the bottom surface (Supporting Information). This asymmetric charge distribution induces a potential across the sample. In the limit of a thin insulator, the maximum potential (and the maximum amount of charging) is set by the band gap of the material; i.e., once the potential is sufficiently large, any additional charging is mitigated by Zener tunneling.[35] Thus, if the flux is sufficiently high, one would expect the charging and potential to saturate, as we observed.

Since these materials charged more than any materials we are aware of (Supporting Information, Video V4), it is important to further understand the underlying charging mechanism. UPS results (Supporting Information, Figure S2) indicated that $DyScO_3$ has a work function of 5.8 eV and the band gap, experimentally measured with REELS (Supporting Information, Figure S2), was found to be 5.7 ± 0.1 eV. These values are in agreement with previously reported values[36,37] and help explain the large charging: the band gap and work function of $DyScO_3$ are approximately equal, so almost every secondary electron produced by inelastic scattering in the bulk has sufficient energy to escape the material. As a direct confirmation of this hypothesis, Figure 3 compares secondary electron images of $GdScO_3$ and $KTaO_3$ nanoparticles.[38,39] As

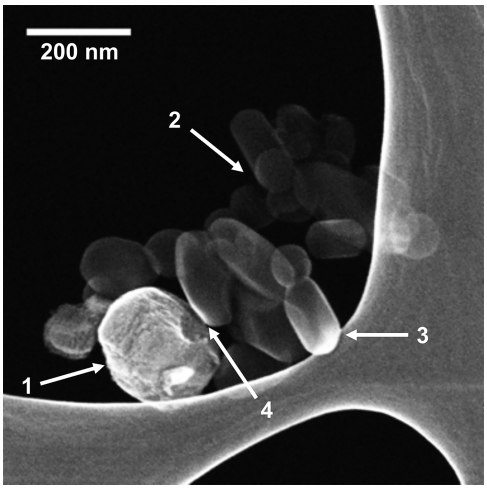

Figure 3. Secondary electron (SE) image of $GdScO_3$ and $KTaO_3$ nanoparticles acquired on a STEM operated at 200 kV. Typically, SE images show strong topographic contrast as shown at 1 for a $KTaO_3$ nanoparticle. Due to charging, $GdScO_3$ nanoparticles have significantly less signal, and the drop in topographic contrast directly connects to a long mean free path for the secondary electrons, such as at 2. In areas where local charge compensation is possible, e.g., near carbon at 3 or less charged $KTaO_3$ nanoparticles at 4, there is enhanced signal in the $GdScO_3$ nanoparticles.

can be seen in this image, the $GdScO_3$ nanoparticles have less topographic contrast than the $KTaO_3$ nanoparticles, and a significantly lower secondary electron signal except near the conducting carbon support or $KTaO_3$ nanoparticles. The lack of topographic contrast directly indicates a long mean free path of the electrons; the lower secondary electron signal is because the $GdScO_3$ has charged significantly more positive than the $KTaO_3$. The relatively short distance over which the contrast from the $GdScO_3$ varies indicates very poor conduction even for the relatively large electric field gradients present.

It is also important to elucidate the role of the surface (and rule out the possibility of an anomalous surface structure or phase which, for instance, could lead to misfit stresses). XPS measurements were used to determine if water was present on the $DyScO_3$ TEM samples, since hydroxides often occur at oxide surfaces and could lead to surface dipoles. Results indicated that the annealed samples prior to TEM experiments had minimal chemisorbed hydroxide (Supporting Information, Figure S3). For the surface structure, the diffraction patterns in Figure 4 show a low diffuse background with no evidence of additional reflections. This indicates few bulk defects and a well-ordered 1 × 1 surface, with no surface reconstructions or additional phases. Based on the annealing conditions, we expect this surface to be valence neutral. AFM imaging (Supporting Information, Figure S4) confirmed that the surface was flat with monatomic steps of a height of 0.15 nm. Angle-resolved XPS measurements indicated that the surface is a Sc rich double-layer dominated by $ScO_5[]$ octahedra with a vacant site (Supporting Information, Figure S4), similar to the well-established double-layer reconstructions on $SrTiO_3$ (001).[40−44] This is anticipated because the 1 × 1 (110) surface of $DyScO_3$ (a *Pbnm* orthorhombic perovskite) is similar to the 2 × 2 (001) surface of a cubic perovskite. DFT calculations performed with the all-electron augmented plane wave and local orbitals WIEN2k code[45] for different surface configurations indicated that the lowest energy structure contained three rows of

DOI: 10.1021/acs.nanolett.8b01126
Nano Lett. 2018, 18, 3850−3856

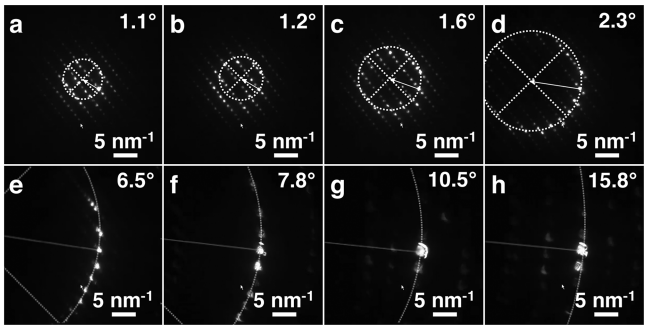

Figure 4. Demonstration of bending of a [110] oriented sample of $DyScO_3$ via electron diffraction. Eight frames of a transmission electron diffraction pattern (Supporting Information, Video V5), which show the sample bending in reciprocal space as the electron flux is decreased from panels a–h. There is no discernible change (±0.1 nm^{-1}) in the distance between the transmitted beam and a stationary reference point (mouse pointer). A solid white arrow is drawn from the transmitted beam to the approximate center of the Laue circle. Tilt angles from the [110] zone axis (top right corner) were estimated by fitting circles to the strong spots on the Laue circle.

scandium oxide (Supporting Information, Figure S5). Except for a small density of unoccupied states associated primarily with one of the surface Sc atoms, there was nothing unusual in the surface band structure, consistent with the experimental UPS and REELS data. These results allow us to exclude anomalous surface structures or phases as the source of the bending and suggest that disordering the surface decreased charging (and therefore bending) because ion-beams will differentially sputter oxygen and lead to a reduced, disordered, and more conductive surface which helps neutralize charging, similar to coating with carbon.

Our TEM observations as well as structural and electronic characterizations were all consistent with the sample bending as a result of a charging-induced potential across the sample, i.e., a converse flexoelectric response. To further establish the origins of the bending, ex situ characterization of the bulk flexoelectric effect in $DyScO_3$ was carried out using a three-point bending method.[9] Polarization versus strain gradient for a [110] oriented $DyScO_3$ sample is shown in Figure 5. To validate the setup, the flexoelectric coefficients of [100] and [110] oriented $SrTiO_3$ were measured to have magnitudes of 12.4 nC/m and 8.3 nC/m, respectively, consistent with literature

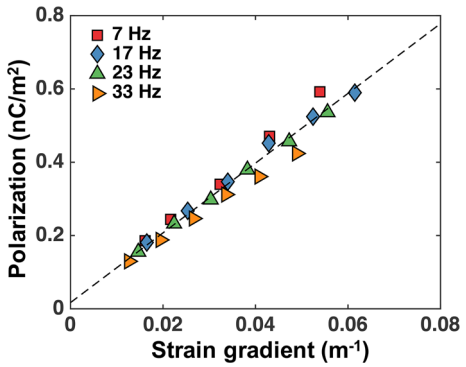

Figure 5. Flexoelectric polarization magnitude versus strain gradient for a series of measurements performed at different oscillatory frequencies for [110] oriented $DyScO_3$. The dashed line indicates a linear fit between strain gradient and polarization. The slope of such a line is the flexoelectric coefficient.

values which range from 1 to 10 nC/m; see ref 9. Flexoelectric coefficients were found to minimally vary with static force and oscillatory frequency. The magnitude of the flexoelectric coefficient for [110] oriented $DyScO_3$ was measured to be 8.4 ± 0.4 nC/m, using the standard error for 13 different measurements. The signs for [110] oriented $DyScO_3$ and $SrTiO_3$ were negative, which agree with the sign of the flexoelectric coefficient deduced from in situ TEM observations (Supporting Information). Although the flexoelectric coefficient in $DyScO_3$ is of the same order of magnitude as the measured flexoelectric coefficient in $SrTiO_3$, the dielectric constant of $DyScO_3$ at room temperature[46] is an order of magnitude smaller than that of $SrTiO_3$.[47] Therefore, the flexocoupling voltage (ratio of the flexoelectric coefficient to the dielectric constant) is an order of magnitude larger in $DyScO_3$ than in $SrTiO_3$ at 42 ± 2 V. This is larger than typical flexocoupling voltages of 1–10 V; see ref 6.

It is possible to quantitatively connect the ex situ flexoelectric measurements with the in situ TEM observations via an expression developed by Bursian and Trunov.[48] Assuming a plate geometry and constant electric field across the thickness of the sample, the curvature is given by $\kappa = \frac{\mu V}{D} = \mu V \frac{12(1-\nu^2)}{Yd^3}$ where κ is the curvature, μ is the flexoelectric coefficient, D is the flexural rigidity, V is the potential, ν is the Poisson's ratio, Y is the Young's modulus, and d is the elastic thickness, which we will take as the sample thickness. Using the measured flexoelectric coefficient, band gap (as discussed previously, once the charging in a thin insulator has saturated, it is reasonable to estimate the saturated potential across the sample with the band gap), literature Young's modulus, and thickness from the in situ observations, we can arrive at an estimate for the curvature arising from the flexoelectric effect in the saturated regime.

First, it is necessary to estimate the elastic thickness to use in this calculation because there are inherent thickness gradients in the TEM samples, and the above expression was derived for a plate of uniform thickness. From the TEM experiments, we found that the thickness in the $DyScO_3$ samples varied from approximately 50 nm at the base of the features (based upon electron energy loss measurements) to 5 nm or less at the edges. Taking an average elastic thickness of 22.5 nm, the measured band gap of 5.7 eV, a Poisson's ratio of 0.25, and a Voigt–Reuss–Hill average[49] for the Young's modulus of 183 GPa, we obtain a curvature of 2.5×10^5 m^{-1}. We note that although the sample is a single crystal with known elastic tensor coefficients, we used the Voigt–Reuss–Hill average to estimate the Young's modulus as it is ambiguous what elastic tensor components it is proper to use for the effective modulus. We argue that the agreement with our observed saturated curvature ($\sim 3 \times 10^5$ m^{-1}) is semiquantitative especially given the approximations made in deriving the above expression[48] and in the thickness and modulus estimations. It is worth noting that estimating the saturated potential across the sample as the band gap corresponds to a surface charge density of 0.3 electrons/nm^2. This is a large, but reasonable, charge density that is seen in a number of other insulating systems.[50]

To verify that these observations were not associated with an electron optics artifact, we collected diffraction patterns while varying the electron flux after tilting to the [110] zone axis of a $DyScO_3$ sample. As shown in Figure 4 (Supporting Information, Video V5) as the electron flux is decreased from panels a–h, changes in the Laue circle indicate that the sample

DOI: 10.1021/acs.nanolett.8b01126
Nano Lett. 2018, 18, 3850–3856

is bending. While there was a slight deflection of the beam, it was several orders of magnitude smaller than the bending of the sample. For completeness, changing the microscope focus did not lead to large shifts in the beam, which is consistent with minimal bending of the electron beam.

A second possibility is that the ∼2 T magnetic fields in the microscope play a role in the observed bending; $DyScO_3$ changes from a paramagnetic to an antiferromagnetic state below 4 K and measurements have shown that a magnetic field of a few T can rotate $DyScO_3$ samples around this transition temperature.[51] We performed experiments in low-field electron microscopes that exposed the samples to ∼5 Oe magnetic fields and observed similar bending (Supporting Information, Figure S6), ruling out magnetic contributions as the dominant term.

A number of other remote possibilities are briefly discussed in the Supporting Information; they are orders of magnitude too small to account for the magnitude of the observed bending. We note that these unlikely effects can also be ruled out as they would have led to bending in other samples of different materials and be well-known in the existing literature.

With nominal strains comparable to or exceeding the yield strains of typical oxides, these experimental observations of reversible bending in lanthanide scandates are quite extraordinary; extraordinary, but consistent with what one expects for the flexoelectric effect at the nanoscale and the large reduction of the flexural rigidity. Theoretical predictions have claimed very large flexoelectric responses should exist at the nanoscale due to how flexoelectricity scales with size; however, prior to this work, there have been no direct observations of such scaling, leaving this size extrapolation open to question. Our results provide direct experimental evidence that this size extrapolation is physically reasonable.

In terms of application, these observations experimentally demonstrate the feasibility of constructing nanoscale devices with quite large mechanical motions relative to their size. In terms of the fundamental science, many questions remain regarding the detailed physical origin of the large flexocoupling voltage in these materials as well as general features of the flexoelectric effect, since it is in many respects the least explored electromechanical coupling. To date, theoretical and experimental studies of flexoelectricity have focused on relatively simple oxides. These lanthanide scandates contain strongly correlated 4f electrons (We note that Dy has two minority 4f electrons in $DyScO_3$, Tb has one in $TbScO_3$, and Gd has none in $GdScO_3$ and all three scandates showed approximately the same bending, so the minority 4f states may play a role, but their presence is not required.), significant octahedral rotations, strong and anomalous polar phonons,[52] as well as other physical terms such as Rashba spin−orbit coupling[53] when electric fields are present and probably additional complex couplings between spin and orbital moments and atomic positions (Supporting Information). They are much more complex systems with rich and, as of yet, relatively unexplored science compared to simpler materials such as $SrTiO_3$ or $BaTiO_3$, where flexoelectric phenomena have been previously studied. Dissecting the interplay between electronic, phonon, and spin−orbit terms in these strongly correlated materials is a challenge which we will pose to the larger community.

■ ASSOCIATED CONTENT

Supporting Information

The Supporting Information is available free of charge on the ACS Publications website at DOI: 10.1021/acs.nanolett.8b01126.

Sample preparation, experimental methods and analysis, density functional theory calculations, charging in an electron microscope, sign of the flexoelectric coefficients, and other possible contributions (PDF)
Video V1 (AVI)
Video V2 (AVI)
Video V3 (AVI)
Video V4 (AVI)
Video V5 (AVI)
Surface structure (CIF)

■ AUTHOR INFORMATION

Corresponding Author

*E-mail: L-marks@northwestern.edu.

ORCID

Christopher A. Mizzi: 0000-0002-4209-854X

Author Contributions

P.K. carried out the electron microscopy, X-ray photoelectron spectroscopy, atomic force microscopy, and reflection electron energy loss spectroscopy measurements and analysis, P.K. and C.M. carried out the ultraviolet photoelectron spectroscopy measurements, and C.M. carried out the ex situ measurements of the flexoelectric coefficient, all under the supervision of L.D.M. L.D.M. carried out the density functional theory calculations. All three authors worked on the manuscript.

Funding

This work was supported by the U.S. Department of Energy, Office of Science, Basic Energy Sciences, under award no. DE-FG02-01ER45945.

Notes

The authors declare no competing financial interest.

■ ACKNOWLEDGMENTS

The authors are indebted to Yimei Zhu of Brookhaven National Laboratory and Amanda Petford-Long of Argonne National Laboratory for heroic assistance with extremely hard to handle samples in their low magnetic field transmission electron microscopes. We thank Ryan Paull for the $GdScO_3$ nanoparticles, Tiffany Ly for the $KTaO_3$ nanoparticles, and Tiffany Ly and Zachary Mansley for the secondary electron images. We would also like to thank Oleg Rubel for information on the Berry Phase calculations as well as unreleased versions of the code BerryPI. We thank Fabien Tran and Peter Blaha for discussions on the use of hybrid functionals in the WIEN2k code, as well as James M. Rondinelli, Kenneth R. Poeppelmeier, and Peter W. Voorhees for their scientific input on the materials. Ex situ flexoelectric measurements were made possible using equipment from L. Catherine Brinson and Lincoln J. Lauhon. This work was supported by the U.S. Department of Energy, Office of Science, Basic Energy Sciences, under award no. DE-FG02-01ER45945.

■ REFERENCES

(1) Bursian, E. V.; Zaikovskii, O. I. Changes in the curvature of a ferroelectric film due to polarization. *Sov. Phys. Solid State* **1968**, *10* (5), 1121−1124.

DOI: 10.1021/acs.nanolett.8b01126
Nano Lett. 2018, 18, 3850−3856

(2) Meyer, R. B. Piezoelectric Effects in Liquid Crystals. *Phys. Rev. Lett.* **1969**, *22* (18), 918−921.
(3) Indenbom, V. L.; Loginov, E. B.; Osipov, M. A. Flexoelectric Effect and Crystal-Structure. *Kristallografiya* **1981**, *26* (6), 1157−1162.
(4) Petrov, A. G. Flexoelectricity of model and living membranes. *Biochim. Biophys. Acta, Biomembr.* **2002**, *1561* (1), 1−25.
(5) Yudin, P. V.; Tagantsev, A. K. Fundamentals of flexoelectricity in solids. *Nanotechnology* **2013**, *24* (43), 432001.
(6) Zubko, P.; Catalan, G.; Tagantsev, A. K. Flexoelectric Effect in Solids. *Annu. Rev. Mater. Res.* **2013**, *43*, 387−421.
(7) Cross, L. E. Flexoelectric effects: Charge separation in insulating solids subjected to elastic strain gradients. *J. Mater. Sci.* **2006**, *41* (1), 53−63.
(8) Narvaez, J.; Vasquez-Sancho, F.; Catalan, G. Enhanced flexoelectric-like response in oxide semiconductors. *Nature* **2016**, *538* (7624), 219−221.
(9) Zubko, P.; Catalan, G.; Buckley, A.; Welche, P. R. L.; Scott, J. F. Strain-gradient-induced polarization in $SrTiO_3$ single crystals. *Phys. Rev. Lett.* **2007**, *99* (16), 167601.
(10) Ma, W.; Cross, L. E. Observation of the flexoelectric effect in relaxor $Pb(Mg_{1/3}Nb_{2/3})O_3$ ceramics. *Appl. Phys. Lett.* **2001**, *78* (19), 2920.
(11) Biancoli, A.; Fancher, C. M.; Jones, J. L.; Damjanovic, D. Breaking of macroscopic centric symmetry in paraelectric phases of ferroelectric materials and implications for flexoelectricity. *Nat. Mater.* **2015**, *14*, 224−229.
(12) Stengel, M. Unified *ab initio* formulation of flexoelectricity and strain-gradient elasticity. *Phys. Rev. B: Condens. Matter Mater. Phys.* **2016**, *93* (24), 245107.
(13) Hong, J.; Vanderbilt, D. First-principles theory and calculation of flexoelectricity. *Phys. Rev. B: Condens. Matter Mater. Phys.* **2013**, *88*, 174107.
(14) Stengel, M. Microscopic response to inhomogeneous deformations in curvilinear coordinates. *Nat. Commun.* **2013**, *4*, 2693.
(15) Tagantsev, A. K. Piezoelectricity and flexoelectricity in crystalline dielectrics. *Phys. Rev. B: Condens. Matter Mater. Phys.* **1986**, *34* (8), 5883−5889.
(16) Resta, R. Towards a bulk theory of flexoelectricity. *Phys. Rev. Lett.* **2010**, *105* (12), 127601.
(17) Hong, J.; Catalan, G.; Scott, J. F.; Artacho, E. The flexoelectricity of barium and strontium titanates from first principles. *J. Phys.: Condens. Matter* **2010**, *22* (11), 112201.
(18) Maranganti, R.; Sharma, P. Atomistic determination of flexoelectric properties of crystalline dielectrics. *Phys. Rev. B: Condens. Matter Mater. Phys.* **2009**, *80*, 054109.
(19) Gharbi, M.; Sun, Z. H.; Sharma, P.; White, K. The origins of electromechanical indentation size effect in ferroelectrics. *Appl. Phys. Lett.* **2009**, *95* (14), 142901.
(20) Robinson, C. R.; White, K. W.; Sharma, P. Elucidating the mechanism for indentation size-effect in dielectrics. *Appl. Phys. Lett.* **2012**, *101* (12), 122901.
(21) Catalan, G.; Sinnamon, L. J.; Gregg, J. M. The effect of flexoelectricity on the dielectric properties of inhomogeneously strained ferroelectric thin films. *J. Phys.: Condens. Matter* **2004**, *16* (13), 2253−2264.
(22) Majdoub, M. S.; Maranganti, R.; Sharma, P. Understanding the origins of the intrinsic dead layer effect in nanocapacitors. *Phys. Rev. B: Condens. Matter Mater. Phys.* **2009**, *79* (11), 115412.
(23) Eliseev, E. A.; Morozovska, A. N.; Svechnikov, G. S.; Maksymovych, P.; Kalinin, S. V. Domain wall conduction in multiaxial ferroelectrics. *Phys. Rev. B: Condens. Matter Mater. Phys.* **2012**, *85* (4), 045312.
(24) Maksymovych, P.; Morozovska, A. N.; Yu, P.; Eliseev, E. A.; Chu, Y.-H.; Ramesh, R.; Baddorf, A. P.; Kalinin, S. V. Tunable Metallic Conductance in Ferroelectric Nanodomains. *Nano Lett.* **2012**, *12* (1), 209−213.
(25) Yudin, P. V.; Tagantsev, A. K.; Eliseev, E. A.; Morozovska, A. N.; Setter, N. Bichiral structure of ferroelectric domain walls driven by flexoelectricity. *Phys. Rev. B: Condens. Matter Mater. Phys.* **2012**, *86* (13), 134102.
(26) Catalan, G.; Lubk, A.; Vlooswijk, A. H.; Snoeck, E.; Magen, C.; Janssens, A.; Rispens, G.; Rijnders, G.; Blank, D. H. A.; Noheda, B. Flexoelectric rotation of polarization in ferroelectric thin films. *Nat. Mater.* **2011**, *10* (12), 963−967.
(27) Eliseev, E. A.; Morozovska, A. N.; Gu, Y. J.; Borisevich, A. Y.; Chen, L. Q.; Gopalan, V.; Kalinin, S. V. Conductivity of twin-domain-wall/surface junctions in ferroelastics: Interplay of deformation potential, octahedral rotations, improper ferroelectricity, and flexoelectric coupling. *Phys. Rev. B: Condens. Matter Mater. Phys.* **2012**, *86* (8), 085416.
(28) Morozovska, A. N.; Eliseev, E. A.; Glinchuk, M. D.; Chen, L. Q.; Gopalan, V. Interfacial polarization and pyroelectricity in antiferrodistortive structures induced by a flexoelectric effect and rotostriction. *Phys. Rev. B: Condens. Matter Mater. Phys.* **2012**, *85* (9), 094107.
(29) Lee, D.; Jeon, B. C.; Yoon, A.; Shin, Y. J.; Lee, M. H.; Song, T. K.; Bu, S. D.; Kim, M.; Chung, J. S.; Yoon, J. G.; Noh, T. W. Flexoelectric control of defect formation in ferroelectric epitaxial thin films. *Adv. Mater.* **2014**, *26* (29), 5005−5011.
(30) Deng, Q.; Kammoun, M.; Erturk, A.; Sharma, P. Nanoscale flexoelectric energy harvesting. *Int. J. Solids Struct.* **2014**, *51* (18), 3218−3225.
(31) Jiang, X. N.; Huang, W. B.; Zhang, S. J. Flexoelectric nano-generator: Materials, structures and devices. *Nano Energy* **2013**, *2* (6), 1079−1092.
(32) Bhaskar, U. K.; Banerjee, N.; Abdollahi, A.; Wang, Z.; Schlom, D. G.; Rijnders, G.; Catalan, G. A flexoelectric microelectromechanical system on silicon. *Nat. Nanotechnol.* **2016**, *11* (3), 263−266.
(33) Huang, W. B.; Yang, S. R.; Zhang, N. Y.; Yuan, F. G.; Jiang, X. N. Direct Measurement of Opening Mode Stress Intensity Factors Using Flexoelectric Strain Gradient Sensors. *Exp. Mech.* **2015**, *55* (2), 313−320.
(34) Lee, D.; Yoon, A.; Jang, S. Y.; Yoon, J. G.; Chung, J. S.; Kim, M.; Scott, J. F.; Noh, T. W. Giant flexoelectric effect in ferroelectric epitaxial thin films. *Phys. Rev. Lett.* **2011**, *107* (5), 057602.
(35) Zener, C. A theory of the electrical breakdown of solid dielectrics. *Proc. R. Soc. London, Ser. A* **1934**, *145* (855), 523−529.
(36) Derks, C.; Kuepper, K.; Raekers, M.; Postnikov, A. V.; Uecker, R.; Yang, W. L.; Neumann, M. Band-gap variation in $RScO_3$ (R = Pr, Nd, Sm, Eu, Gd, Tb, and Dy): X-ray absorption and O K-edge x-ray emission spectroscopies. *Phys. Rev. B: Condens. Matter Mater. Phys.* **2012**, *86* (15), 155124.
(37) Mizzi, C. A.; Koirala, P.; Marks, L. D. Electronic structure of lanthanide scandates. *Phys. Rev. Mater.* **2018**, *2*, 025001.
(38) Ly, T.; Wen, J.; Marks, L. D. Kinetic Growth Regimes of Hydrothermally Synthesized Potassium Tantalate Nanoparticles. *Nano Lett.*, submitted for publication, **2018**.
(39) Paull, R. J.; Mansley, Z. R.; Ly, T.; Marks, L. D.; Poeppelmeier, K. R. Synthesis of Gadolinium Scandate from a Hydroxide Hydrogel. *Inorg. Chem.* **2018**, *57* (7), 4104−4108.
(40) Erdman, N.; Marks, L. D. $SrTiO_3$ (001) surface structures under oxidizing conditions. *Surf. Sci.* **2003**, *526* (1−2), 107−114.
(41) Erdman, N.; Poeppelmeier, K. R.; Asta, M.; Warschkow, O.; Ellis, D. E.; Marks, L. D. The structure and chemistry of the TiO_2-rich surface of $SrTiO_3$ (001). *Nature* **2002**, *419* (6902), 55−58.
(42) Erdman, N.; Warschkow, O.; Asta, M.; Poeppelmeier, K. R.; Ellis, D. E.; Marks, L. D. Surface Structures of $SrTiO_3$ (001): A TiO_2-rich Reconstruction with a c(4 × 2) Unit Cell. *J. Am. Chem. Soc.* **2003**, *125* (33), 10050−10056.
(43) Kienzle, D. M.; Becerra-Toledo, A. E.; Marks, L. D. Vacant-Site Octahedral Tilings on $SrTiO_3$(001), the (13 × 13)R33.7° Surface, and Related Structures. *Phys. Rev. Lett.* **2011**, *106* (17), 176102.
(44) Lanier, C. H.; van de Walle, A.; Erdman, N.; Landree, E.; Warschkow, O.; Kazimirov, A.; Poeppelmeier, K. R.; Zegenhagen, J.; Asta, M.; Marks, L. D. Atomic-scale structure of the $SrTiO_3$(001)−c(6 × 2) reconstruction: Experiments and first-principles calculations. *Phys. Rev. B: Condens. Matter Mater. Phys.* **2007**, *76* (4), 045421.

DOI: 10.1021/acs.nanolett.8b01126
Nano Lett. 2018, 18, 3850−3856

(45) Blaha, P.; Schwarz, K.; Madsen, G.; Kvasnicka, D.; Luitz, J. *WIEN2k: An Augmented Plane Wave Plus Local Orbitals Program for Calculating Crystal Properties*; Technische Universität Wien: Wien, Austria, 2001.
(46) Coh, S.; Heeg, T.; Haeni, J. H.; Biegalski, M. D.; Lettieri, J.; Edge, L. F.; O'Brien, K. E.; Bernhagen, M.; Reiche, P.; Uecker, R.; Trolier-McKinstry, S.; Schlom, D. G.; Vanderbilt, D. Si-compatible candidates for high-K dielectrics with the *Pbnm* perovskite structure. *Phys. Rev. B: Condens. Matter Mater. Phys.* **2010**, *82*, 064101.
(47) Neville, R. C.; Hoeneisen, B.; Mead, C. A. Permittivity of Strontium Titanate. *J. Appl. Phys.* **1972**, *43*, 2124.
(48) Bursian, E.; Trunov, N. Nonlocal piezoelectric effect. *Sov. Phys. Solid State* **1974**, *16*, 760−762.
(49) Chung, D. H. Elastic Moduli of Single Crystal and Polycrystalline MgO. *Philos. Mag.* **1963**, *8* (89), 833−841.
(50) Bernardini, F.; Fiorentini, V.; Vanderbilt, D. Spontaneous polarization and piezoelectric constants of III-V nitrides. *Phys. Rev. B: Condens. Matter Mater. Phys.* **1997**, *56* (16), No. R10024(R).
(51) Ke, X.; Adamo, C.; Schlom, D. G.; Bernhagen, M.; Uecker, R.; Schiffer, P. Low temperature magnetism in the perovskite substrate $DyScO_3$. *Appl. Phys. Lett.* **2009**, *94* (15), 152503.
(52) Kamba, S.; Goian, V.; Nuzhnyy, D.; Bovtun, V.; Kempa, M.; Prokleska, J.; Bernhagen, M.; Uecker, R.; Schlom, D. G. Polar phonon anomalies in single-crystalline $TbScO_3$. *Phase Transitions* **2013**, *86* (2−3), 206−216.
(53) Manchon, A.; Koo, H. C.; Nitta, J.; Frolov, S. M.; Duine, R. A. New perspectives for Rashba spin−orbit coupling. *Nat. Mater.* **2015**, *14*, 871−882.

DOI: 10.1021/acs.nanolett.8b01126
Nano Lett. 2018, 18, 3850−3856